Local and Average Structure in Zinc Cyanide: Toward an Understanding of the Atomistic Origin of Negative Thermal Expansion

Simon J. Hibble,*,[†] Ann M. Chippindale,*,[†] Elena Marelli,[†] Scott Kroeker,*,[‡] Vladimir K. Michaelis,[‡,⊥] Brandon J. Greer,[‡] Pedro M. Aguiar,[§] Edward J. Bilbé,[†] Emma R. Barney,[∥,#] and Alex C. Hannon*,[∥]

[†]Department of Chemistry, University of Reading, Whiteknights, Reading RG6 6AD, United Kingdom
[‡]Department of Chemistry, University of Manitoba, Winnipeg, Manitoba R3T 2N2, Canada
[§]Department of Chemistry, University of York, York YO10 5DD, United Kingdom
[∥]ISIS Facility, Rutherford Appleton Laboratory, Chilton, Didcot OX11 0QX, United Kingdom

S *Supporting Information*

ABSTRACT: Neutron diffraction at 11.4 and 295 K and solid-state ^{67}Zn NMR are used to determine both the local and the average structures in the disordered, negative thermal expansion (NTE) material, $Zn(CN)_2$. Solid-state NMR not only confirms that there is head-to-tail disorder of the C≡N groups present in the solid, but yields information about the relative abundances of the different $Zn(CN)_{4-n}(NC)_n$ tetrahedral species, which do not follow a simple binomial distribution. The $Zn(CN)_4$ and $Zn(NC)_4$ species occur with much lower probabilities than are predicted by binomial theory, supporting the conclusion that they are of higher energy than the other local arrangements. The lowest energy arrangement is $Zn(CN)_2(NC)_2$. The use of total neutron diffraction at 11.4 K, with analysis of both the Bragg diffraction and the derived total correlation function, yields the first experimental determination of the individual Zn−N and Zn−C bond lengths as 1.969(2) and 2.030(2) Å, respectively. The very small difference in bond lengths, of ∼0.06 Å, means that it is impossible to obtain these bond lengths using Bragg diffraction in isolation. Total neutron diffraction also provides information on both the average and the local atomic displacements responsible for NTE in $Zn(CN)_2$. The principal motions giving rise to NTE are shown to be those in which the carbon and nitrogen atoms within individual Zn−C≡N−Zn linkages are displaced to the same side of the Zn···Zn axis. Displacements of the carbon and nitrogen atoms to opposite sides of the Zn···Zn axis, suggested previously in X-ray studies as being responsible for NTE behavior, in fact make negligible contributions at temperatures up to 295 K.
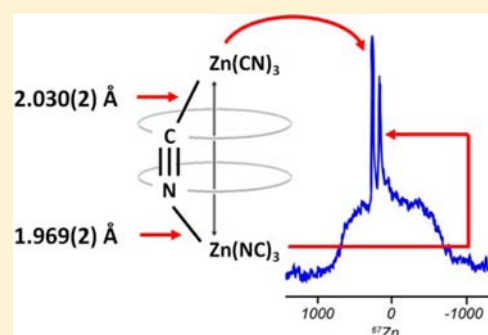
INTRODUCTION

Zinc cyanide (Figure 1) has attracted much interest because it is a three-dimensional negative thermal expansion (NTE) material; that is, its volume decreases with increasing temperature. Furthermore, it exhibits a relatively large NTE effect with a thermal expansion coefficient, α_l, of -16.9×10^{-6} K^{-1} over the temperature range 25−375 K.[1] One challenge in the study of this material is its disordered nature. Williams et al.[2] showed using neutron Bragg diffraction that head-to-tail cyanide disorder exists in this compound, and the average structure is best described in space group $Pn\bar{3}m$, in contrast to previously proposed ordered models in $P\bar{4}3m$.[3] However, Williams et al.[2] were unable to determine the individual Zn−C and Zn−N bond lengths and the relative populations of the five possible $Zn(CN)_{4-n}(NC)_n$ local arrangements (Figure 2).

In their study of $Zn(CN)_2$ using total X-ray diffraction and pair distribution function analysis (PDF), Chapman et al.[4] proposed two mechanisms to explain NTE, which arise from two distinct motions (Figure 3). These are here referred to as skipping-rope and kinky motions (Figure 3a and b), respectively. In our study of one-dimensional NTE in AgCN using neutron diffraction and total correlation function analysis,[5] we found that the skipping-rope motion of the type shown in Figure 3a is the predominant cause of contraction in the $[Ag−C≡N−]_n$ chains over the temperature range 10−300 K. However, for $Zn(CN)_2$, Chapman et al.[4] reached no conclusion regarding which type of motion is responsible for the NTE. In addition, the C≡N distances in the cyanide units derived from their X-ray data are physically unrealistic and vary unreasonably rapidly with temperature. At 297 K, their two models produced C≡N bond lengths of 1.399 and 1.305 Å for the kinky and skipping-rope modes, respectively, rather larger than the commonly accepted value of 1.15 Å found in a range of transition-metal cyanides (Supporting Information Table S.16). The smaller X-ray form factors for carbon and nitrogen
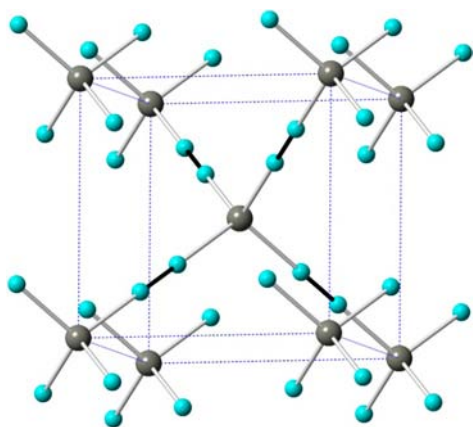
Figure 1. The structure of $Zn(CN)_2$ in space group $Pn\bar{3}m$. Key: zinc atoms, gray spheres; head-to-tail disordered cyanide, cyan spheres.

Figure 3. The two possible transverse displacements of the C and N atoms from their average atomic positions in a linear Zn−C≡N−Zn linkage previously proposed to account for NTE in zinc cyanide: (a) a skipping-rope (or smooth) mode in which the C and N are displaced to the same side of the Zn⋯Zn axis (parallel motion) and (b) a kinky mode in which the C and N are displaced on opposite sides of the axis (antiparallel motions). The horizontal lines are aids to the eye to show how modes (a) and (b) result in a contraction of the Zn⋯Zn distance.

as compared to that of zinc means that it would have been impossible for Chapman et al.[4] to determine directly the C≡N bond distances from an X-ray atomic pair correlation experiment. Thus, the deficiency of their models might not have been immediately apparent. A further discrepancy in the paper of Chapman et al.[4] is that the value for the *a* lattice parameter obtained from Bragg X-ray diffraction over a 100−400 K temperature range appears to be inaccurate and is significantly longer than those measured by a number of other research groups (Supporting Information Figure S.2). A very recent synchrotron X-ray study of the structure of $Zn(CN)_2$ as a function of pressure[6] found that at 1.52 GPa, it undergoes a phase transition from the cubic ($Pn\bar{3}m$) form to an orthorhombic (*Pbca*) form, $Zn(CN)_2$-II. In $Zn(CN)_2$-II, the Zn−C≡N−Zn linkage is no longer on average linear, as in the cubic polymorph, but forms two types of bent unit, one of which is of the skipping-rope type as shown in Figure 3a with the distortions remaining mainly in the plane. The second distortion is more severe and involves kinking of the type shown in Figure 3b combined with buckling out of the plane. Other recent work by Werner-Zwanziger et al.[7] uses solid-state NMR methods on ^{13}C and ^{15}N enriched zinc cyanide to show that the C≡N bond length must be less than or equal to 1.19(1) Å, casting further doubt on the earlier work of Chapman et al.[4]

A particularly powerful way to study the structure of disordered transition-metal cyanides and the structural origin of NTE behavior in these materials is to use total neutron diffraction.[5,8−12] This method yields both the total correlation function and the Bragg diffraction. In favorable cases, the correlation function can be analyzed to yield model-independent bond lengths and the variation in these bond lengths (root-mean square (RMS) deviations) arising from thermal motions. Conventional crystallographic analysis of the Bragg component of the total neutron diffraction gives the
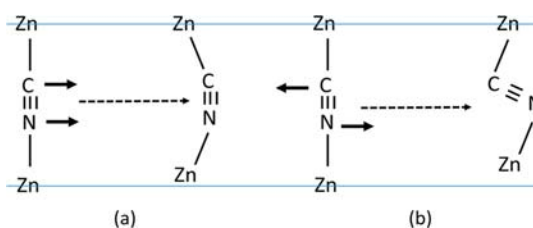
lattice parameters, atomic coordinates, and anisotropic displacement parameters. Combining results from the total correlation function with those from Bragg diffraction can yield information on the local distortions giving rise to NTE. Such analysis of neutron data is not limited to metal cyanides and has been used for studying NTE in oxide materials, for example, ZrW_2O_8[13] and SiO_2,[14,15] which like $Zn(CN)_2$, have structures based on the diamandoid lattice.

A total neutron diffraction study of zinc cyanide in particular has many advantages over X-ray studies. This is because the similar magnitudes of the coherent neutron scattering lengths of zinc, carbon, and nitrogen ($\bar{b}_{Zn}$ = 5.68, $\bar{b}_C$ = 6.646, $\bar{b}_N$ = 9.36 fm)[16] mean that all of the pair correlations make a significant contribution to the total correlation function. One consequence is that the C≡N bond length can be determined directly from the total neutron correlation function. However, the total neutron correlation function does not provide enough information when used in isolation to determine the individual values of the Zn−C and Zn−N bond lengths, which although similar are anticipated to be different, but must be used in conjunction with Bragg neutron diffraction. Although diffraction methods are powerful, a local probe, such as NMR, is required to determine the distribution of C and N atoms in the local zinc coordination sphere in this disordered material. Zinc cyanide contains two identical interpenetrating zinc−cyanide networks. It should be noted that in this work, we focus on the behavior of an individual zinc−cyanide network and do not consider any possible effects of inter-network interactions on NTE.

In $Cd(CN)_2$, which is isostructural with $Zn(CN)_2$, ^{113}Cd (I = 1/2) NMR showed that all of the possible local arrangements in the $Cd(CN)_{4−n}(NC)_n$ species are found (as shown for $Zn(CN)_2$ in Figure 2).[17] The relative intensities of the ^{113}Cd NMR resonances arising from the different species closely resemble those observed for the $Cd(CN)_2$ framework in the related cadmium−cyanide clathrate, $Cd(CN)_2 \cdot C_6H_{12}$, which
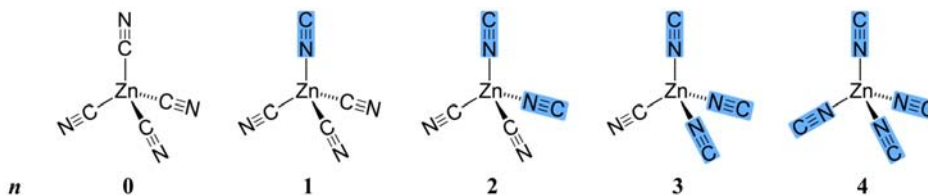
Figure 2. The five distinct species in $Zn(CN)_{4−n}(NC)_n$ clusters arising from head-to-tail disorder of the C≡N groups.

yield a population distribution for the species Cd-$(CN)_4$:Cd-$(CN)_3(NC)$:$Cd(CN)_2(NC)_2$:$Cd(CN)(NC)_3$:$Cd(NC)_4$ of 2.0 : 22.8 : 50.3 : 23.2 : 1.7, which is significantly different from the binomial distribution of 6.25 : 25.00 : 37.50 : 25.00 : 6.25. The conclusion reached is that the $Cd(CN)_4$ and $Cd(NC)_4$ species have significantly higher energies than the other species and that $Cd(CN)_2(NC)_2$ lies at the lowest energy, in agreement with the first-principle electronic structure calculations of Ding et al.[18] In contrast, their calculations found no significant energy differences between the $Zn(CN)_{4-n}(NC)_n$ species in $Zn(CN)_2$. If this conclusion were correct, one would predict a binomial distribution for these species.

Despite its apparent attractiveness for directly probing local order and connectivity in $Zn(CN)_2$, ^{67}Zn NMR is far from routine. With its low magnetogyric ratio ($\gamma = 1.68 \times 10^7$ rad $T^{-1}\ s^{-1}$), sizable quadrupole moment ($Q = 150$ mb; $I = 5/2$), and meager natural abundance (4.1%), ^{67}Zn is generally considered a "difficult" NMR nuclide for solid-state studies,[19] and there are few reports of its use in the literature.[20−27] Most successful ^{67}Zn NMR studies are carried out at very high magnetic fields to mitigate the effects of quadrupolar coupling and to enhance sensitivity. In recent NMR work, Werner-Zwanziger et al.[7] demonstrated the application of ^{67}Zn NMR to $Zn(CN)_2$ and were able to confirm that there is structural disorder in this material. Two sharp ^{67}Zn NMR signals were ascribed to $Zn(CN)_4$ and $Zn(NC)_4$ species, and a broad signal was assigned to the remaining $Zn(CN)_{4-n}(NC)_n$ species. However, the relative abundances of the different species were not determined.

In this Article, we use ultrahigh-field ^{67}Zn NMR data, supported by quantum chemical calculations of quadrupole coupling constants, C_Q, and asymmetry parameters, η, to determine the relative populations of the five possible $Zn(CN)_{4-n}(NC)_n$ species (Figure 2). This study reveals that, as is found in $Cd(CN)_2$,[17] the population of the local metal species, $M(CN)_{4-n}(NC)_n$, does not follow a binomial distribution. The quantum chemical calculations also suggest that the Zn−N bond length should be shorter than the Zn−C bond length. In addition, we determine experimentally, using total neutron diffraction, the structural nature of the transverse mode responsible for NTE in zinc cyanide. The skipping-rope mode (Figure 3a) is a good description of the local distortions, which produce a contraction in the a lattice parameter on heating, and the kinky motion (Figure 3b) is shown to be unimportant. Total neutron diffraction also reveals that the Zn−N bond length is indeed shorter than the Zn−C bond length. At 11.4 K, the Zn−N and Zn−C bond lengths differ by 0.061 Å and are found to be 1.969(2) and 2.030(2) Å, respectively.

■ RESULTS AND DISCUSSION

^{67}Zn NMR. The ^{67}Zn NMR spectrum of nonspinning $Zn(CN)_2$ acquired at 21.1 T presents as two sharp peaks situated atop a relatively featureless broad signal (Figure 4). A fully ordered structure, as proposed by Hoskins and Robson in space group $P\bar{4}3m$,[3] would contain only two zinc species, $Zn(CN)_4$ and $Zn(NC)_4$, in the ratio 1:1. These would both have perfect T_d symmetry, and therefore there would be no quadrupolar broadening of the ^{67}Zn NMR signals. The presence of significant intensity in the broad underlying resonance is incompatible with this model, as previously discussed.[7] To understand the origin of the broad signal, it is necessary to consider the effects of quadrupole coupling on the
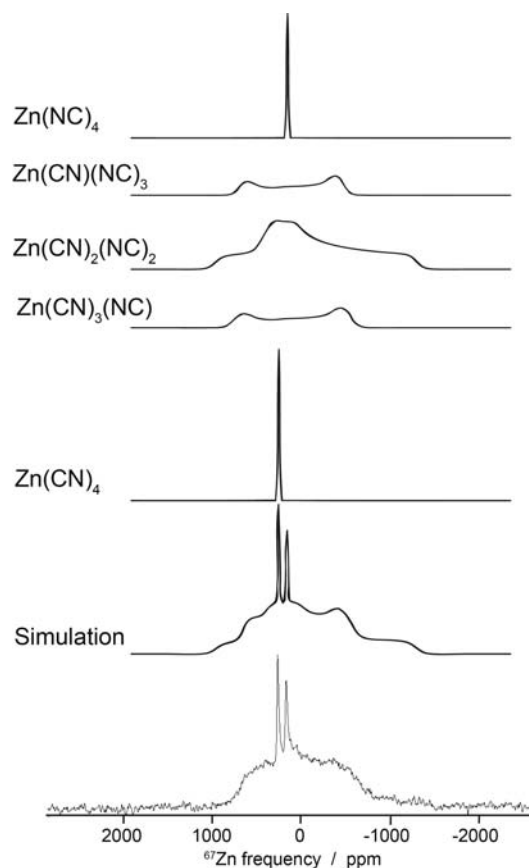

Figure 4. ^{67}Zn NMR spectrum of solid $Zn(CN)_2$ at 21.1 T and the best-fit simulation. The contributions to the simulated spectrum of the individual species, $Zn(CN)_{4-n}(NC)_n$, are shown above.

^{67}Zn NMR peak shapes. The coupling of the nuclear electric quadrupole moment, eQ, of the ^{67}Zn nucleus with the electric-field gradient of the surrounding lattice, eq, in the presence of a dominant external magnetic field produces broadening of the NMR peaks. Only in the case of cubic symmetry, such as in a fully ordered $Zn(CN)_2$ structure in $P\bar{4}3m$, will the electric field gradient be zero, producing two unbroadened resonances. The electric field gradients arising from the $Zn(CN)(NC)_3$, $Zn(CN)_2(NC)_2$, and $Zn(CN)_3(NC)$ species will lead to nonzero quadrupole coupling constants, $C_Q = (eQ)(eq)/h$, and the correspondingly broad resonance features observed. Hence, the experimental NMR spectrum presents unambiguous evidence that a significant number of zinc atoms are surrounded by mixtures of C and N atoms, and therefore head-to-tail cyanide disorder is present in solid $Zn(CN)_2$.

In principle, the inherently quantitative nature of NMR spectroscopy provides the means to assess the relative populations of each of the five possible Zn coordination environments present in the $Zn(CN)_{4-n}(NC)_n$ species (Figure 2). Indeed, the sharpness and resolution of the peaks corresponding to the symmetrical $Zn(CN)_4$ and $Zn(NC)_4$ species, at 275 and 175 ppm, permit reliable integrated intensities to be measured, representing 3.5% and 2.5% of the total ^{67}Zn NMR signal, respectively. These peak assignments are based on our GIPAW-calculated magnetic isotropic shieldings, σ_{iso} (Table 1), and ^{67}Zn MAS NMR spectral features (see Supporting Information, section S.2). Calculations predict successive chemical shift differences of −21, −32, −42, and −47 ppm between pairs of species $Zn(CN)_{4-n}(NC)_n$ and

Table 1. Experimental Parameters Used in Fitting the Nonspinning ^{67}Zn NMR Spectrum of Zn(CN)$_2$, along with Corresponding Computed Values

	experimental				hybrid DFT[b]		GIPAW[c]		
fragment	C_Q/MHz	η	δ_{iso}/ppm[a]	intensity/%	C_Q/MHz	η	C_Q/MHz	η	σ_{iso}[d]
Zn(CN)$_4$	1.2 ± 0.2	<0.2	275 ± 3	3.5 ± 0.1	0.75	0.05	0	0	1268.13
Zn(NC)(CN)$_3$	11.0 ± 1.0	<0.3	250 ± 30	(15)[e]	12.65	0.07	12.56	0	1289.24
Zn(NC)$_2$(CN)$_2$	11.5 ± 1.0	0.85 ± 0.10	220 ± 30	64 ± 5	14.20	0.86	13.69	0.88	1321.60
Zn(NC)$_3$(CN)	10.5 ± 1.0	<0.3	200 ± 30	(15)[e]	14.65	0.08	14.00	0	1363.38
Zn(NC)$_4$	1.2 ± 0.2	<0.2	175 ± 3	2.5 ± 0.1	1.21	0.04	0	0	1410.92

[a]Chemical shifts measured relative to 1 M Zn(NO$_3$)$_2$ (aq). [b]Hybrid DFT method using B3LYP hybrid functional within Gaussian 03 and aug-cc-pVQZ basis set. [c]GIPAW method within CASTEP using full geometry optimization of a single unit cell at the fine level. [d]Calculated isotropic shieldings have not been converted to chemical shifts due to the lack of an appropriate reference compound; note that magnetic shielding values increase in the direction opposite to that of experimental chemical shifts. [e]The similarity of the lineshapes of these two sites precludes the determination of their individual intensities. The overall integrated intensity of the two sites is 30 ± 5, which has been partitioned on the assumption of equal contributions from Zn(NC)(CN)$_3$ and Zn(NC)$_3$(CN).

Zn(CN)$_{4-(n+1)}$(NC)$_{n+1}$ for n = 0, 1, 2, and 3, respectively. This is consistent with the relative ordering of the Cd(NC)$_4$ and Cd(CN)$_4$ sites in ^{113}Cd MAS NMR of Cd(CN)$_2$, but differs from the peak assignments proposed by Werner-Zwanziger et al.[7] for Zn(CN)$_2$. Even without assigning the peaks, our measurements show that only ~6% of the Zn nuclei in the sample are present in Zn(CN)$_4$ and Zn(NC)$_4$ environments (Table 1).

Although relative intensities obtained from NMR experiments are routinely equated with relative site populations, the quadrupolar interaction introduces several factors that must be taken into account when producing accurate relative population values. Fortuitously, in this case, SIMPSON calculations[28] show that the corrections necessary to convert intensities to populations in the ^{67}Zn NMR spectrum for Zn(CN)$_2$ are extremely small and within the experimental errors in the determined intensities (see Supporting Information, section S.3). Hence, we use the experimentally determined relative intensities as measures of the relative populations for the five Zn(CN)$_{4-n}$(NC)$_n$ species.

In chemical terms, the Zn(CN)$_4$ and Zn(NC)$_4$ species in Zn(CN)$_2$ can be described as having T_d symmetry, and, indeed, this appears to be a good description of the local structure for NMR purposes. Thus, the values C_Q = 1.2 MHz and η < 0.2 for the Zn(CN)$_4$ and Zn(NC)$_4$ sites imply only minor deviations from high site symmetry (i.e., effective symmetry close to T_d or C_{3v}). However, as zinc cyanide is disordered, in crystallographic terms, Zn(CN)$_4$ and Zn(NC)$_4$ species must have C_1 symmetry. That the experimentally determined value of C_Q is not zero confirms that there is no long-range C≡N order in the solid and that the space group describing the average structure must be $Pn\bar{3}m$ rather than $P\bar{4}3m$. The values found for C_Q and the asymmetry parameter, η, for the Zn(CN)$_4$ and Zn(NC)$_4$ species are in good agreement with those calculated using hybrid DFT and GIPAW methods (see Supporting Information, section S.2).

The breadth and lack of resolution of the NMR signal intensities corresponding to the Zn(CN)(NC)$_3$, Zn-(CN)$_2$(NC)$_2$, and Zn(CN)$_3$(NC) local environments make it very difficult to extract precise populations for these species. Moreover, the dearth of experimental ^{67}Zn NMR and nuclear quadrupole resonance (NQR) studies leaves little choice but to use theoretical calculations to predict C_Q values for the Zn(CN)(NC)$_3$, Zn(CN)$_2$(NC)$_2$, and Zn(CN)$_3$(NC) species. Hybrid-DFT calculations on model clusters and GIPAW calculations using periodic boundary conditions predict a

large increase in the C_Q values for the Zn(CN)(NC)$_3$, Zn(CN)$_2$(NC)$_2$, and Zn(CN)$_3$(NC) species relative to those of the Zn(CN)$_4$ and Zn(NC)$_4$ species (Table 1; see Supporting Information, section S.2). This result is in general agreement with similar calculations by Werner-Zwanziger et al.[7] The C_Q values were used as initial estimates in the fitting of the complete NMR spectrum. Table 1 shows both the theoretical and the experimentally determined parameters. It is also possible to extract the Zn−N and Zn−C bond lengths from the energy-minimized clusters produced in the GIPAW calculations (see Supporting Information, section S.2). These calculations yield the result that the Zn−N bond length is shorter than that of Zn−C, in agreement with the neutron diffraction studies (vide infra).

Simulations of the individual components of the NMR spectrum arising from each of the five possible Zn coordination environments (Figure 2), together with their sum, are shown above the experimental spectrum in Figure 4. These simulations confirm that the two signals from the Zn(CN)(NC)$_3$ and Zn(CN)$_3$(NC) species are broad and virtually indistinguishable. Hence, although the total intensity contribution of the Zn(CN)(NC)$_3$ and Zn(CN)$_3$(NC) species can be estimated with reasonable reliability, it is impossible to place much confidence in their relative populations. Although the signal arising from the Zn(CN)$_2$(NC)$_2$ species is also broad, it exhibits a distinctly different shape and width from the signals of the Zn(CN)(NC)$_3$ and Zn(CN)$_3$(NC) species, and hence its population can be determined with greater certainty (Table 1).

The populations of the Zn(CN)$_{4-n}$(NC)$_n$ species may be compared to those expected on the basis of a binomial distribution (Table 2). Clearly, the symmetrical zinc species, Zn(CN)$_4$ and Zn(NC)$_4$, are significantly lower in occurrence than would be predicted if all bonding arrangements had the same energy. This leads to the conclusion that the energies of the Zn(CN)$_4$ and Zn(NC)$_4$ species are higher than those with zinc bonded to both carbon and nitrogen. Furthermore, Zn(NC)$_4$ is less populous than Zn(CN)$_4$, indicating that it is the highest-energy zinc site in this compound. A similar conclusion was drawn for Cd(NC)$_4$ sites in Cd(CN)$_2$ (Table 2).[17] In addition, the Zn(CN)$_2$(NC)$_2$ species has a much higher population than would be predicted by a binomial distribution, showing that its energy is significantly lower than those of the other species. It is notable that the theoretical treatment of Cd(CN)$_2$ by Ding et al.[18] produced significant energy differences between the structures based on different

Table 2. Comparison of Relative Populations of the Different Coordination Environments, $M(CN)_{4-n}(NC)_n$, in $Zn(CN)_2$ and the $Cd(CN)_2$ Framework in $Cd(CN)_2 \cdot C_6H_{12}$

	measured populations/%		
local arrangement in $M(CN)_2$	M = Zn	M = Cd[17]	binomial distribution of populations[a]/%
$M(CN)_4$	3.5	2.0	6.25
$M(NC)(CN)_3$	15	22.8	25.00
$M(NC)_2(CN)_2$	64	50.3	37.50
$M(NC)_3(CN)$	15	23.2	25.00
$M(NC)_4$	2.5	1.7	6.25

[a]Expected relative populations if all local arrangements have the same energy.

local arrangements of $Cd(CN)_{4-n}(NC)_n$ species, in line with the distribution of local species observed experimentally by NMR.[17] Their theoretical treatment of $Zn(CN)_2$ produced no significant energy differences between the different $Zn(CN)_{4-n}(NC)_n$ species.

Neutron Bragg Diffraction. The lattice parameter, a, for $Zn(CN)_2$, determined by neutron Bragg diffraction, contracts from 5.9463(7) Å at 11.4 K to 5.908(3) Å at 295 K. These values are in good agreement with those determined by Goodwin and Kepert,[1] Williams et al.,[2] and Reckeweg and Simon[29] over a similar range of temperatures (Figure 5 and Supporting Information Figure S.2). It is notable that the values determined by Chapman et al.[4] over the temperature range 100−400 K lie on a curve, which although of a similar form, is displaced to significantly higher values of a than that produced using our data and that of Goodwin and Kepert[1] (Figure 5). The value of the NTE coefficient, $\alpha_l = -22.7 \times 10^{-6}$ K^{-1}, derived from our lattice parameters obtained at 11.4 and 295 K, is slightly greater in magnitude than values quoted by other workers (typically -16.9×10^{-6} K^{-1}),[1] who determine α_l over a different temperature range (25−375 K). This arises because, as Figure 5 shows, α_l is temperature-dependent.

Rietveld structure refinements were carried out for $Zn(CN)_2$ in space groups $P\bar{4}3m$ and $Pn\bar{3}m$ for both the 11.4 and the 295 K neutron data sets. Details of the refinements are given in Supporting Information Tables S.4−S.10. The results confirm previous workers' conclusions[2] that the model in space group $Pn\bar{3}m$, with C and N disordered on the same site, gives a better description of the average structure than one in the alternative space group, $P\bar{4}3m$, which would have, by symmetry, to contain ordered arrangements of $Zn(CN)_4$ and $Zn(NC)_4$ groups. The superiority of models in $Pn\bar{3}m$ is shown by both the lower R-factors obtained using this space group as compared to those in $P\bar{4}3m$ at both 11.4 and 295 K (Supporting Information Table S.4) and the fact that structure refinements of ordered models in $P\bar{4}3m$ yield significantly different displacement parameters for carbon and nitrogen, rather than the expected near equal values for atoms of such similar mass. The displacement parameters in $P\bar{4}3m$ are much lower for carbon than for nitrogen at both 11.4 and 295 K, despite $\bar{b}_c < \bar{b}_N$, suggesting that C and N are disordered on the same site, further pointing to an average-structure description in $Pn\bar{3}m$ being more appropriate. Bragg diffraction shows that there is C/N disorder around the zinc atoms, but cannot yield quantitative information on the distribution of the $Zn(CN)_{4-n}(NC)_n$ species in the zinc coordination sphere, hence the importance of the NMR experiments described above.
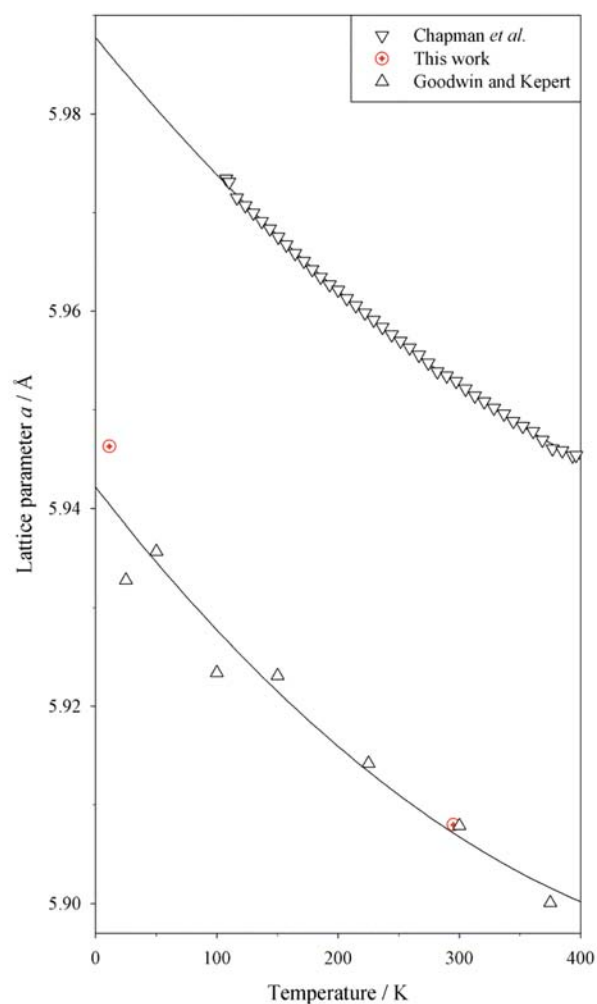

Figure 5. The temperature-dependence of the lattice parameter, a, of $Zn(CN)_2$. The upper line is a quadratic fit to the data of Chapman et al.,[4] while the lower line is a quadratic fit to the data in this work, together with those of Goodwin and Kepert.[1]

Where information obtained from Bragg diffraction can be exploited is in the determination of structural parameters impacting on NTE. Of particular importance are the atomic displacement parameters. Accurate atomic displacement parameters can only be obtained from Bragg diffraction data if careful corrections are made for absorption and multiple diffraction.[30,31] Such corrections are not routinely carried out prior to Bragg analysis, but are essential in total diffraction studies of the type described below. The data used in this work were corrected for these effects before Bragg and total diffraction analyses were attempted.

The anisotropic displacement parameters for C/N in $Pn\bar{3}m$, U_{ii} and U_{ij}, are found from Rietveld refinement (Supporting Information Tables S.6 and S.9). The eigenvalues of the anisotropic displacement tensors yield values for $U_\perp$ and $U_\parallel$, corresponding to motions perpendicular and parallel to the $Zn-C\equiv N-Zn$ axis (Supporting Information Table S.12). The relative values of $U_\perp$ and $U_\parallel$ show that the motion of the $-C\equiv N-$ group is principally perpendicular to the $Zn-C\equiv N-Zn$ axis at both 11.4 and 295 K (Figure 6 and Supporting Information Figure S.6). This is physically reasonable when one considers the relative ease of bond bending motions as compared to bond stretching. It is the bending motions that
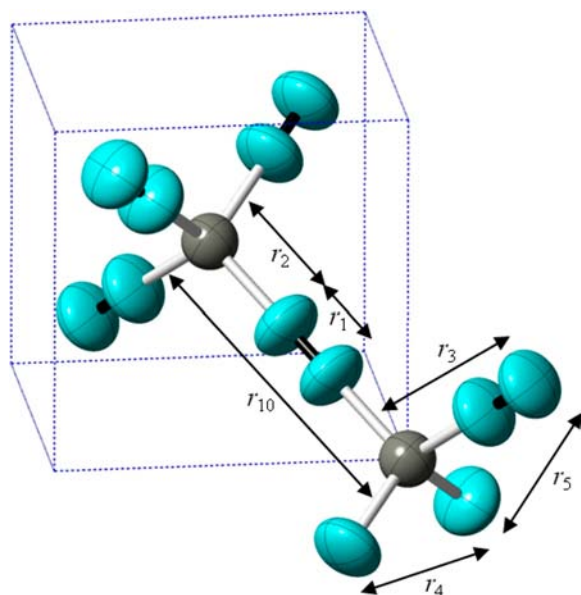
Figure 6. Two linked $Zn(C/N)_4$ tetrahedra in $Zn(CN)_2$, showing the five shortest interatomic correlations, r_1-r_5 (referred to in Table 3), and the first intra-network $Zn \cdots Zn$ correlation, r_{10} (key as for Figure 1). The anisotropic displacement ellipsoids are those at 295 K shown at the 90% level.

produce the transverse movements of the C and N atoms in the $Zn-C\equiv N-Zn$ unit, which correspond to the configurations in

Figure 3a and b postulated to account for NTE behavior. The NTE effect is large even at low temperature, as seen in Figure 5, as transverse motions of the carbon and nitrogen atoms are greater than perpendicular motions even at 11.4 K (Supporting Information Table S.12).

In this work, even at 11.4 K, the C/N displacements perpendicular to the $Zn-C\equiv N-Zn$ axis ($U_\perp = 0.013$ Å^2) are found to be larger than the corresponding parallel motions ($U_\parallel = 0.0094$ Å^2). This is physically reasonable, in contrast to the values of $U_\parallel$ and $U_\perp$ from the results of other workers who found that at low temperatures (14 K (neutron),[2] 25 K (X-ray),[1] and 108 K (X-ray)[4]), $U_\parallel$ is greater than $U_\perp$. These other workers ascribed their results to a possible difference in $Zn-C$ and $Zn-N$ bond lengths. In the case of Williams et al.,[2] a bond-length difference of >0.2 Å would be necessary to account for the values of $U_\parallel$ and $U_\perp$, 0.015 and 0.001 Å^2, derived from their neutron results. This bond-length difference is implausibly large: analysis of bond lengths in ordered materials containing $Zn-C$ and $Zn-N$ bonds yields a bond-length difference of $2.018 - 1.966 = 0.052$ Å (see Supporting Information, section S.12), which in turn would make a contribution of only 0.0007 Å^2 to the displacement parameter, $U_\parallel$, parallel to the $Zn-C\equiv N-Zn$ axis. Combining the results of Bragg and total neutron diffraction, we are able to determine both the magnitude of the difference in the $Zn-N$ and $Zn-C$ bond lengths and the individual bond lengths in disordered $Zn(CN)_2$ (vide infra).

Bond lengths reported in the literature normally represent the differences between average atomic positions and take no account of the correlations of the motions of the bonded pair of

Table 3. Principal Interatomic Correlations in $Zn(CN)_2$ at 11.4 and 295 K Obtained Directly from Total Neutron Diffraction (r_{p-q}) with RMS Variation in Interatomic Distance, $\langle u_{p-q}^2 \rangle^{1/2}$, Together with the Corresponding Distances between the Average Atom Positions Determined from Rietveld Refinement, (r^0_{p-q}), and Their Upper and Lower Limits

			11.4 K		295 K	
	atom pair ($p-q$)		r_{p-q}/Å[b]	$\langle u_{p-q}^2 \rangle^{1/2}$/Å	r_{p-q}/Å[b]	$\langle u_{p-q}^2 \rangle^{1/2}$/Å
total neutron diffraction	$C\equiv N$	(r_1)[a]	1.1510(3)	0.0277(5)	1.1502(3)	0.0294(5)
	$Zn-C/N$	(r_2)	1.9914(5)	0.0555(6)	1.9955(6)	0.0672(7)
		$(r_1 + r_2)$	3.142(1)		3.146(1)	
	$Zn \cdots C/N$	(r_3)	3.150(2)	0.055(1)	3.144(3)	0.070(2)
	$Zn \cdots Zn$	$(r_1 + 2r_2)$	5.134(3)		5.141(3)	
	$(C/N) \cdots (C/N)$	(r_4)	3.239(1)	0.109(2)	3.255(3)	0.147(3)

			11.4 K		295 K	
	atom pair ($p-q$)		r^0_{p-q}/Å[b]	limits/Å[c]	r^0_{p-q}/Å[b]	limits/Å[c]
Rietveld refinement	$C\equiv N$	(r^0_1)	1.1868(7)	1.2087 (↑↓) 1.1868 (↑↑)	1.173(2)	1.272 (↑↓) 1.173 (↑↑)
	$Zn-C/N$	(r^0_2)	1.9814(4)	1.9927 (↑↓) 1.9815 (↑↑)	1.972(1)	2.019 (↑↓) 1.973 (↑↑)
	$Zn \cdots C/N$	(r^0_3)	3.168(2)	3.175 (↑↓) 3.168 (↑↑)	3.145(6)	3.174 (↑↓) 3.145 (↑↑)
	$Zn \cdots Zn$	(r^0_{10})	5.1497(5)	5.1534 (↑↓) 5.1497 (↑↑)	5.116(3)	5.130 (↑↓) 5.116 (↑↑)
	lattice parameter/Å	(a)	5.9464(6)		5.908(3)	

[a]The labels (r_n) refer to correlations shown in Figure 6. [b]r_{p-q} corresponds to the mean instantaneous interatomic distance between the atoms p and q from total neutron diffraction, and r^0_{p-q} is the distance between mean interatomic positions of atoms p and q derived from Rietveld analysis. [c]The bounds of the instantaneous bond lengths are derived from Rietveld analysis using the method of Busing and Levy[32] (see Supporting Information, section S.7). The upper and lower limits correspond to antiparallel (↑↓) and parallel (↑↑) motions of atoms p and q, respectively, and are calculated for comparison with the r_{p-q} values.

atoms. By applying the method of Busing and Levy[32] to the results of Rietveld analysis, limiting values of average instantaneous bond lengths for pairs of atoms can be produced (Table 3) (see Supporting Information, section S.7). When applied to the determination of the C≡N bond length, the lower limit corresponds to correlated parallel C/N displacements perpendicular to the Zn−C≡N−Zn axis (i.e., the skipping-rope mode shown in Figure 3a), and the upper limits correspond to correlated antiparallel displacements perpendicular to the Zn−C≡N−Zn axis (i.e., the kinky mode shown in Figure 3b). Thus, a preliminary conclusion can be reached as to the relative feasibility of the two motions suggested by Chapman[4] (Figure 3) to account for the microscopic motions occurring in $Zn(CN)_2$, which may give rise to NTE. Antiparallel motions of the carbon and nitrogen atoms as shown in Figure 3b lead to average instantaneous bond lengths of 1.209 and 1.272 Å at 11.4 and 295 K, respectively. Clearly antiparallel motions lead to ludicrous C≡N bond lengths, and kinky motions of the type shown in Figure 3b can be ruled out from making a significant contribution to NTE behavior. Parallel motions of the carbon and nitrogen atoms (Figure 3a) however yield values for the C≡N bond length of 1.187 and 1.173 Å at 11.4 and 295 K, respectively. These values are much closer to the expected value of ~1.15 Å, suggesting that the skipping-rope motions are important for NTE. It should be noted at this point that the instantaneous C≡N bond length of 1.187 Å, corresponding to parallel displacements of C and N, is a little longer than the expected value of ~1.15 Å. The reason for this discrepancy is explained later in the discussion of total neutron diffraction, which gives directly the average instantaneous C≡N bond length.

Total Diffraction. The neutron interference function, $Qi^N(Q)$, at 11.4 and 295 K, and the X-ray interference function at 295 K, are shown for $Zn(CN)_2$ in Supporting Information Figure S.8. The neutron and X-ray correlation functions, $T^N(r)$ and $T^X(r)$ (Figure 7), were obtained by Fourier transformation of the corresponding interference functions using the Lorch modification function[33] with a maximum momentum transfer, Q_{max}, of 51.5 and 19.5 Å^{-1} for neutron diffraction and X-ray diffraction, respectively. The first three peaks at short distances in $T^N(r)$ (Figure 7) correspond to atomic pair correlations shown in Figure 6 (see also Supporting Information Table S.11). The first peak in $T^N(r)$ corresponding to $r_1 \approx 1.15$ Å can be unambiguously assigned to the C≡N distance, while the peak corresponding to $r_2 \approx 1.99$ Å, observed in both neutron and X-ray total diffraction studies, is due to short correlations from carbon and nitrogen directly bonded to zinc. The peak manifold at ~3.15 Å is due to two different contributions, that is, the second Zn···C/N distance in the Zn−C≡N−Zn linkage (r_3), and the (C/N)···(C/N) correlation, corresponding to the edge of the $Zn(C/N)_4$ tetrahedron (r_4). Unphysical features at distances shorter than 1 Å do not arise from interatomic distances, but instead are caused by long-wavelength artifacts in the experimental data.[34] The effect of these artifacts diminishes rapidly as r increases, as can be seen in the very low noise level between the peaks in $T^N(r)$ above 0.5 Å. The X-ray total correlation function, $T^X(r)$, was obtained in this work from a laboratory X-ray diffractometer (Figure 7). It should be noted that it is impossible to determine the C≡N bond length using total X-ray diffraction, from either an in-house or synchrotron source,[4] because of the small size of the C and N X-ray form factors relative to that of Zn. Thus, in $T^X(r)$ (Figure 7), there is no peak corresponding to the C≡N correlation seen at ~1.15
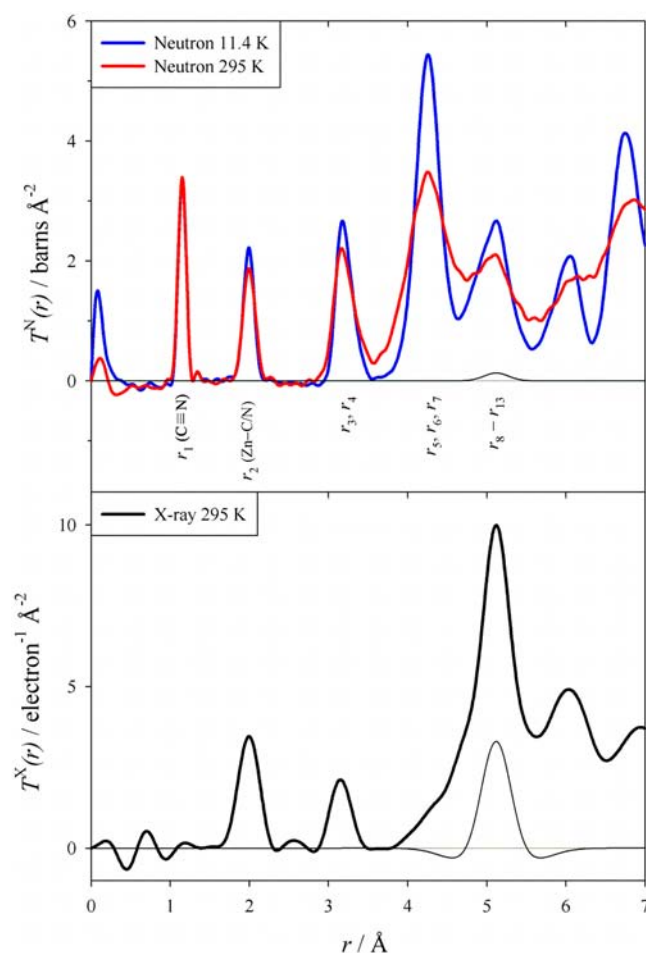

Figure 7. The total correlation function of $Zn(CN)_2$, measured by neutron diffraction, $T^N(r)$, at 11.4 and 295 K (upper frame), and by X-ray diffraction, $T^X(r)$, at 295 K (lower frame). Peaks are labeled with their constituent components corresponding to r_1−r_{13}, the interatomic correlations shown in Figure 6 and Supporting Information Table S.11. The thin black line in each frame shows that the contribution at 295 K from the Zn···Zn correlation in a Zn−C≡N−Zn linkage overlaps with other correlations, and hence the Zn···Zn distance is obtained from Bragg diffraction as described in the text.

Å in $T^N(r)$. It can also be seen in Figure 7 that it is difficult to determine the Zn···Zn distance from $T^X(r)$ as there are other interatomic correlations that make highly significant contributions in this region.

The first three assigned peaks in $T^N(r)$ at both 11.4 and 295 K (Figure 8) were fitted[35] to give the structural parameters shown in Table 3 and Supporting Information Table S.13. The first peak corresponds to the C≡N correlation and was fitted using a single distance. The second peak, which includes both Zn−C and Zn−N correlations, shows no obvious asymmetry and was also initially fitted using a single distance. The third peak was fitted as the sum of two overlapping contributions, Zn···C/N and (C/N)···(C/N) correlations, respectively, with the associated coordination numbers fixed at their ideal crystallographic values. It should be noted that as the coherent neutron scattering lengths of carbon, nitrogen, and zinc are of similar magnitude,[16] all atom pairs make a significant contribution to $T^N(r)$. Thus, total neutron diffraction enables the C≡N bond length to be directly determined with high accuracy, with values of 1.1510(3) and 1.1502(3) Å at 11.4 and 295 K, respectively. A correct measurement of the C≡N bond
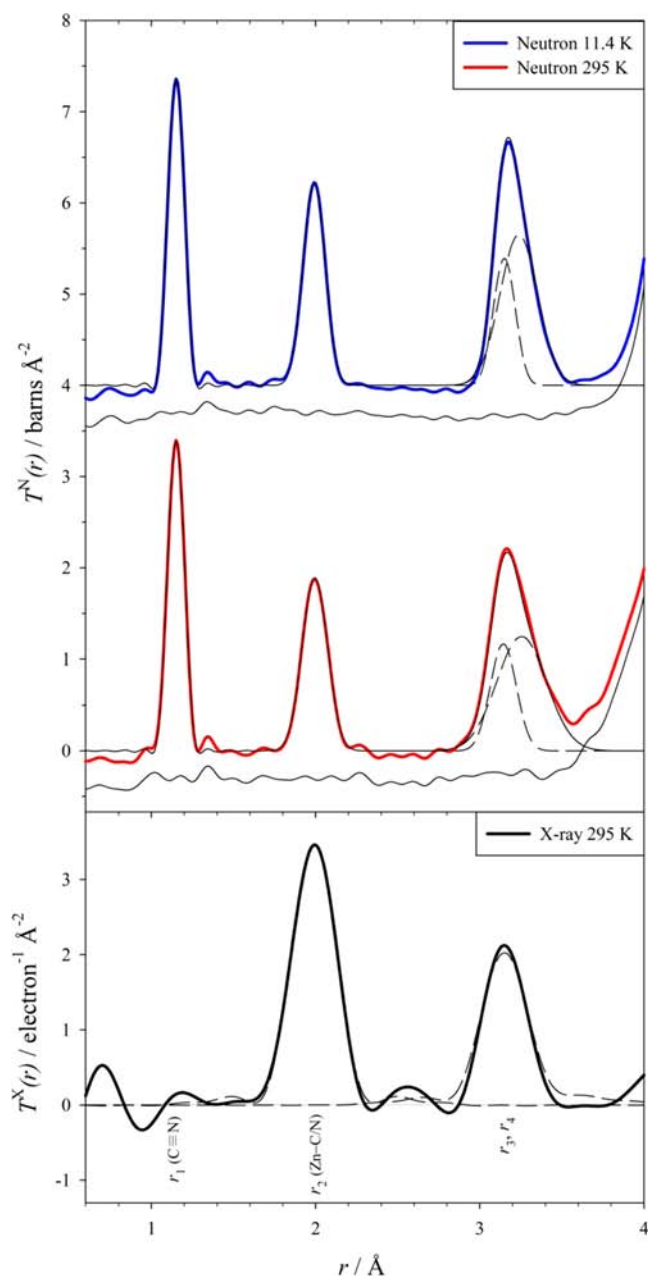
Figure 8. Peak fits to $T^{N}(r)$ at 11.4 and 295 K (upper frame). The individual components (correlations r_3 and r_4) of the third peak are shown by dashed lines, and the residual is shown by a displaced continuous line (see parameters in Table 3 and Supporting Information Table S.13). For $T^{X}(r)$ at 295 K (lower frame), the dashed lines indicate a partial fitting of r_2, r_3, and r_4 (see parameters in Supporting Information Table S.14).

length is essential for determination of the exact structural nature of the NTE behavior in $Zn(CN)_2$. Direct determination of the C≡N bond length is not possible using total X-ray diffraction because the X-ray form factors of C and N are much smaller than Zn, and hence only atom pairs that involve zinc (i.e., Zn···Zn and Zn−C/N) make a significant contribution to $T^{X}(r)$ (Figure 8). Lacking this information and placing no constraints on the C≡N bond length, Chapman et al.[4] were unable to discriminate between the different mechanisms they proposed for NTE in $Zn(CN)_2$ using X-ray data.

Combination of Total Neutron Diffraction and Rietveld Analysis. Table 3 shows a comparison of the internuclear distances obtained from fitting the total neutron correlation functions and those derived from the Rietveld structure refinements.[36] A combination of the information from the two techniques is required to provide insights into the motions responsible for NTE in $Zn(CN)_2$ and detailed structural information, the Zn−C and Zn−N bond lengths.

The C≡N bond length obtained from fitting $T^{N}(r)$ is the true average of the different C≡N distances in $Zn(CN)_2$ (as the cyanide groups bridging the five different $Zn(CN)_{4-n}(NC)_n$ species (Figure 2) might be expected to have slightly different C≡N bond lengths). In contrast, the C≡N distance derived from Rietveld analysis, $r^0_{C≡N}$, represents the distance between the mean positions of the carbon and nitrogen atoms. The difference between the C≡N bond lengths obtained using the two techniques cannot be accounted for merely by atomic motions; that is, the values directly determined by total neutron diffraction at both 11.4 and 295 K lie outside the limits on the mean instantaneous bond lengths derived from Rietveld data using the method of Busing and Levy[32] (Table 3).

The reason the derived C≡N bond length from Rietveld analysis, $r^0_{C≡N}$, is in error is that the C and N atoms do not lie on exactly the same average atomic position, as has been assumed during refinement. This produces a value of the C≡N bond length longer than the true value determined from total diffraction. The discrepancy can be accounted for if, as is actually the case (vide infra), the atomic position of N lies closer to that of Zn than does that of C. Because the coherent neutron scattering length of nitrogen is substantially greater than that of carbon,[16] the mean position of C/N lies closer to the Zn atom than the true mean position, and hence the derived C≡N distance is longer than the true value as determined using total neutron diffraction. This error in the determination of the true average C/N position also means that the Zn−C/N distance is too short when determined from Rietveld analysis.

The $T^{N}(r)$ data were initially analyzed by assuming that the Zn−N and Zn−C bonds have the same length, a reasonable assumption as there is no evident asymmetry in the peak ascribed to these correlations ($r_2 \approx 1.99$ Å). However, a consequence of this assumption is that the sum of the average instantaneous bond lengths in the Zn−C≡N−Zn linkage, derived from $(r_1 + 2r_2)$, at 11.4 K is less than the zinc to zinc distance, Zn···Zn. This is a physical impossibility as the shortest distance between two points is a straight line. The origin of this discrepancy is that, as in the case of the Rietveld analysis, different scattering lengths for C and N result in the determined mean Zn−C/N distance being slightly too short. We show below, by combining results from $T^{N}(r)$ and Bragg diffraction, that the Zn−N bond is shorter than the Zn−C bond and calculate the individual bond lengths in this disordered material.

Using the values of r_1 and r_2 from total diffraction (Table 3) and the Zn···Zn distance in the Zn−C≡N−Zn linkage from Rietveld analysis (as peak overlap means that an accurate Zn···Zn distance cannot be obtained from $T^{N}(r)$ or $T^{X}(r)$, Figure 7), and assuming that the linkage is linear, allows a first estimate for the individual Zn−N ($d_{Zn−N}$) and Zn−C ($d_{Zn−C}$) bond lengths to be obtained from the relationships:

$$r_2 = \frac{\bar{b}_N d_{Zn−N} + \bar{b}_C d_{Zn−C}}{\bar{b}_N + \bar{b}_C} \tag{1}$$

and

$$d_{Zn-N} + d_{Zn-C} + r_1 = d_{Zn \cdots Zn} \qquad (2)$$

This method, using a Zn⋯Zn distance of 5.1497 Å, yields values of Zn−N = 1.952 Å and Zn−C = 2.047 Å.

The finding from this simple approach that the Zn−N bond length is shorter than that of Zn−C agrees with crystal-structure determinations of ordered mixed-metal cyanides (see Supporting Information, section S.12) and also with the theoretical results of Ding et al. for $Zn(CN)_2$.[18] However, the difference in the bond lengths of 0.095 Å is larger than the value of 0.052(14) Å found between the mean of the previously determined values for Zn−N (1.966(12) Å) and the Zn−C value (2.018(7) Å) in the mixed-metal cyanides.

A more sophisticated approach, as described in Supporting Information, section S.10, was therefore adopted in which the assumption that the Zn−C and Zn−N distances are different was incorporated in the initial peak fitting procedure rather than extracting this information from the position of the second peak in $T^N(r)$ at ~1.99 Å after fitting. In addition, in this approach, the first three peaks were fitted simultaneously (see Supporting Information, section S.10). Again, the conclusion is reached that Zn−N is shorter than Zn−C, but the values obtained, 1.969(2) and 2.030(2) Å, and their difference, 0.061(2) Å, are slightly different from the ones found in the simpler treatment. As this approach makes the ab initio assumption that the Zn−N and Zn−C bond lengths are distinct, we believe that these bond lengths are the more reliable.

In the simplified approach, it was assumed that the Zn−C≡N−Zn linkage is linear, and even using the more sophisticated approach, it proved impossible to incorporate transverse motions when fitting the low-temperature data. This is because the transverse motions are so small at 11.4 K that they produce only small effects (0.003 Å) on the calculated bond lengths (see Supporting Information, section S.11). These changes in the bond lengths are of the same order as the errors in the bond lengths found in the full peak fitting treatment.

The approximation that the Zn−C≡N−Zn linkage is linear is only reasonable at low temperature, where the atom displacements are small. The situation is very different at 295 K. At this temperature, the transverse motions of C and N are very significant (Supporting Information Table S.12), and consequently the Zn⋯Zn distance in the Zn−C≡N−Zn linkage, calculated from $(r_1 + 2r_2)$, is much greater than the true Zn⋯Zn distance determined from Rietveld analysis of the Bragg diffraction (Table 3). Detailed analysis of the size of this difference allows the nature of the transverse modes responsible for NTE to be determined.

It should be noted that at high temperature, it is not possible to extract simultaneously the individual Zn−C and Zn−N bond lengths and derive the size of the transverse motions by fitting the first three peaks of the total diffraction data. Hence, the Zn−C bond length used is that obtained by analysis of the 11.4 K $T^N(r)$ data. At high temperature, the transverse C and N motions are large and extractable from a combination of the 295 K $T^N(r)$ data and the true Zn⋯Zn distance, determined from Rietveld analysis. It is impossible to fit models based on the kinky mode shown in Figure 3b. Using the skipping-rope model (Figure 3a) (see Supporting Information, section S.10) yielded the structural parameters shown in Supporting Information Table S.15, with the corresponding fit to $T^N(r)$ shown in Supporting Information Figure S.11. The transverse

displacement found for C and N at 295 K, Δ = 0.266(4) Å, obtained from this fit to $T^N(r)$ is in good agreement with the value of 0.241 Å obtained from Rietveld analysis for the displacement of C and N perpendicular to the Zn−C≡N−Zn linkage (Supporting Information Table S.12).

The same conclusion, that is, that the skipping-rope modes are the predominant transverse motion, is even reached on ignoring the difference between the Zn−C and Zn−N bond lengths and using the value of r_2 from Table 3 (Supporting Information Figure S.13). Using this approximation, the calculated value of Δ is 0.223 Å, which differs only slightly from those above. It is clear therefore that the skipping-rope mode, Figure 3a, gives a good description of the atomic displacements in $Zn(CN)_2$, which lead to a contraction of the Zn⋯Zn distance with temperature and accounts for the NTE behavior of this material. In contrast, the kinky mode, Figure 3b, is incompatible with the data. This can be shown in a number of different ways. For example, using the value of r_2 for the Zn−C/N bond length, together with the Zn⋯Zn distance in the Zn−C≡N−Zn linkage and the C and N displacements obtained from Rietveld analysis, which do not prejudge whether the motion is skipping-rope type or kinky, it is possible to calculate what $d_{C≡N}$ would have to be if this distortion occurred (Supporting Information Figure S.14). Using Δ = 0.241 Å yields $d_{C≡N}$ = 1.251 Å. This value for $d_{C≡N}$ is clearly incompatible with the value of $d_{C≡N}$ = 1.1502(3) Å found directly from $T^N(r)$ at 295 K and the values of $d_{C≡N} \approx 1.15$ Å found in related ordered cyanides (see Supporting Information, section S.12).

All of the above analysis only considers motions in which all four atoms in the Zn−C≡N−Zn linkage remain in one plane. At first sight, this might appear to be an unrealistic simplification as zinc cyanide is a three-dimensional framework material. The skipping-rope planar mode is, in fact, a very good description of the microscopic atomic behavior responsible for NTE. Any motion into the third dimension involves mixing a proportion of the planar kinky mode with the predominant skipping-rope mode. As illustrated in Figure 9, on average
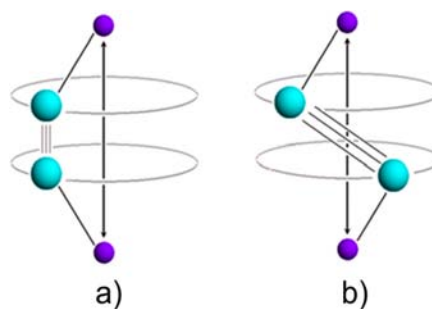

Figure 9. Schematic diagrams showing (a) the planar skipping-rope mode in the Zn−C≡N−Zn linkage drawn in three dimensions and (b) an admixture of a small fraction of the kinky mode with the skipping-rope mode, which produces an unfeasibly long C≡N distance and illustrates why kinky modes can be discounted in the explanation of NTE.

within the structure this fraction can only be very small as the planar skipping-rope mode fits the experimental data so well. This conclusion is in agreement with the results of inelastic neutron scattering studies and ab initio calculations of the phonon dispersion curves in $Zn(CN)_2$.[37] In the work of Mittal et al.,[37] the modes with negative Grüneisen parameters, that is,

the modes responsible for NTE, involve predominantly displacements of C and N to the same side of the Zn···Zn axis, as required in the skipping-rope-mode model. These modes occur at low energy and so will be significantly populated up to room temperature.

So far, the motions of the Zn atoms have not been discussed, even though it is clear from the Rietveld refinement that they move significantly, albeit less than the C and N atoms. Our analysis above does not preclude zinc motion, and indeed it is possible from our results to reach some conclusions regarding the relative motions of nearest-neighbor zinc atoms. We do not attempt to obtain information on long-range correlations, for example, correlated motions around the six-ring shown in Supporting Information Figure S.7. We might however expect on physical grounds that the low-energy acoustic modes would result in the motions of nearest-neighbor zinc lying much closer to the parallel than the antiparallel limits. In Table 3, the limits on the average instantaneous Zn···Zn distance at 11.4 and 295 K arising from parallel and antiparallel Zn atom motions are reported. These values are calculated by combining the distance between the average zinc positions with information on isotropic displacement parameters. As the calculations in Supporting Information section S.11 show, using the parallel limits leads to excellent agreement between the calculated C and N displacements and the experimentally determined anisotropic displacement parameters, confirming that nearest-neighbor zinc atoms are displaced in parallel, or nearly so.

Figure 9a illustrates the average instantaneous form of the Zn−C≡N−Zn linkages; that is, the linkages will nearly always be bent and hardly ever straight. However, as the degree of bend in the Zn−C≡N−Zn linkages changes, as they flex, the zinc atoms will be dragged backward and forward but constrained by symmetry to move within the spheres seen in Figure 6. It seems likely that, although $Cd(CN)_2$ is isostructural with $Zn(CN)_2$, a more complex explanation for NTE might be necessary as the recent study by Fairbank et al.[38] examining diffuse X-ray scattering in single crystals of $Cd(CN)_2$ shows that complex Cd displacements take place below room temperature. This is in line with the fact that $Cd(CN)_2$ undergoes a phase transition at low temperature.[1]

■ CONCLUSIONS

Combining the results of neutron Bragg diffraction, total diffraction, and analysis of solid-state ^{67}Zn NMR has produced new experimentally determined information on the local structure in zinc cyanide and the precise nature of the transverse modes responsible for the NTE behavior of this material.

An important aspect of this work is that the C≡N bond length in zinc cyanide is determined directly and precisely using total neutron diffraction via the correlation function. This contrasts with previous results obtained using total X-ray diffraction. Knowledge of the C≡N bond length is one of the key pieces of information required if meaningful information on the structural distortions leading to NTE is to be extracted from diffraction data.

The results obtained on combining the two neutron diffraction techniques show that the Zn−N and Zn−C bond lengths are different and have values of 1.969(2) and 2.030(2) Å, respectively, at 11.4 K. The very small bond length difference of 0.061 Å in this disordered material can only be determined using this combined approach. Theoretical studies are in agreement with our experimental results: for $Zn(CN)_2$ (and

$Cd(CN)_2$), density functional calculations previously predicted that M−N bonds are shorter than M−C bonds.[18] Recently, we used Reverse Monte Carlo modeling to fit simultaneously the Bragg neutron and total correlation function, $T^N(r)$, for $Ni(CN)_2$.[39] Once again, the M−N bond was found to be shorter than the M−C bond, with the Ni−N bond being 0.046 Å shorter than the Ni−C bond.

It is tempting to think that the fact that the Zn−N bond length is shorter than the Zn−C bond length in this disordered form of zinc cyanide might be used to assign C and N to specific sites in the recently characterized high-pressure form, $Zn(CN)_2$-II.[6] Currently, this structure is described with C/N disorder on all of the nonmetal sites, even though the four Zn−C/N bond lengths fall into two sets with two shorter bonds at 1.906 and 1.917 Å and two longer at 1.961 and 1.957 Å. Assuming that the shorter bonds can be assigned to Zn−N and the longer to Zn−C, we suggest that cyanide groups in zinc cyanide order at high pressure.

The difference in bonding of the two ends of the bridging −C≡N− group is also reflected in the fact that the distribution of $Zn(CN)_{4-n}(NC)_n$ local coordination possibilities does not follow the binomial distribution expected if bonding to the carbon and nitrogen is equivalent. Solid-state ^{67}Zn NMR shows that the $Zn(CN)_2(NC)_2$ arrangement occurs much more frequently, 64(5)%, than expected statistically (37.5%), and the $Zn(CN)_4$ and $Zn(NC)_4$ species much less frequently with observed frequencies of 3.5(1)% and 2.5(1)% versus the binomial expectations of 6.25% for both of these species. These results are consistent with the $Zn(CN)_2(NC)_2$ having the lowest energy of the five possible arrangements, as was found for $Cd(CN)_2$ from both NMR experiments[17] and quantum mechanical calculations.[18] Given that our sample was made by recrystallization, it is likely to be the thermodynamic product. It is possible that samples of $Zn(CN)_2$ with different distributions of $Zn(CN)_{4-n}(NC)_n$ species might be accessible if kinetic control could be used in their preparation. We are currently investigating if this is indeed possible.

It is notable that both the theoretical calculations on ordered models of $Zn(CN)_2$ by Ding et al.[18] and our quantum chemical calculations carried out on supercells containing a pseudo-random distribution of $Zn(CN)_{4-n}(NC)_n$ species both predict that Zn−N bonds are shorter than Zn−C bonds. However, in all cases, the bond-length difference is less than the value of 0.061 Å we find experimentally here. In addition, the calculations of Ding et al.[18] do not produce energy differences between the different $Zn(CN)_{4-n}(NC)_n$ arrangements to reproduce the distribution found here experimentally.

It is almost self-evident that transverse modes are responsible for the NTE behavior in $Zn(CN)_2$. However, the exact nature of these modes has not previously been determined experimentally. Using neutron Bragg diffraction and total neutron correlation function in combination, motions in the Zn−C≡N−Zn linkage involving displacements of C and N atoms to opposite sides of the bridge, that is, kinky modes, are ruled out from making a contribution to NTE behavior. NTE behavior in zinc cyanide is found to be a result of motion of C and N to the same side of the Zn−C≡N−Zn axis, that is, skipping-rope modes. Such a mode corresponds to one of the distortions found when zinc cyanide is transformed to the high-pressure form, $Zn(CN)_2$-II.[6]

■ EXPERIMENTAL SECTION

Sample Preparation. Caution! Cyanide materials can be toxic and must be handled with care.

50 g of commercial $Zn(CN)_2$ (Aldrich, 98% pure) was recrystallized from 200 mL of ammonia solution (0.88/35% aqueous). The resulting white powder was dried under vacuum at 60 °C for 4 h and shown to be phase pure using powder X-ray diffraction. Prior to the neutron diffraction experiment, the sample was further dried under vacuum at 110 °C for 1 week to remove any hydrogenous impurities, which, if present, would give rise to a large and unmanageable background for neutron diffraction. The density of the purified material, measured using a Quantachrome micropycnometer at room temperature with helium gas as the working fluid, was 1.900(5) g cm^{-3}, in good agreement with the values of 1.886 and 1.891 g cm^{-3} determined at room temperature from single-crystal X-ray diffraction[29] and Rietveld analysis of neutron diffraction (Supporting Information Table S.4), respectively. This accurately measured density was used to correct the total X-ray and neutron diffraction data.

IR and Raman spectra were collected at room temperature from undiluted powders using a Perkin-Elmer Spectrum 100 FT-IR spectrometer with a Universal Attenuated Total Reflection sampling accessory and a Renishaw InVia Raman microscope ($\lambda_{exc} = 785$ nm), respectively (Supporting Information Figures S.15 and S.16). The $\overline{\nu}_{C\equiv N}$ stretching frequency occurred at 2216 cm^{-1} in both spectra with a $\overline{\nu}_{Zn-C/N}$ stretching frequency at 335 cm^{-1} also visible in the Raman spectrum, in good agreement with previously reported values.[40,41]

Nuclear Magnetic Resonance. ^{67}Zn NMR data were acquired using a Bruker Avance II 900 (21.1 T) spectrometer with a 7 mm magic-angle spinning probe. The spectrum was acquired using a quadrupole-echo pulse sequence with 3 μs $\pi/2$ pulses calibrated using a 1 M aqueous solution of $Zn(NO_3)_2$ ($\nu_{rf} = 28$ MHz), an echo delay of 600 μs, an optimized relaxation delay of 5 s, and 43 100 scans. The frequency axis was referenced to 0 ppm 1 M $Zn(NO_3)_2$ (aq). The spectrum was simulated using WSOLIDS,[42] with isotropic chemical shifts (δ_{iso}), quadrupolar couplings (C_Q), and quadrupolar asymmetry parameters (η) based on direct observation or inferences from quantum chemical calculations.

Quantum Chemical Calculations. Quantum chemical calculations using hybrid-DFT (B3LYP) and GIPAW (Gauge Including Projector Augmented Waves) methods were performed within Gaussian 03[43] and CASTEP[44] software packages, respectively, on a series of model clusters constructed from diffraction data to represent the five possible $Zn(CN)_{4-n}(NC)_n$ species (see Supporting Information, section S.2).

Neutron Diffraction Experiments. Neutron diffraction patterns of $Zn(CN)_2$ were measured at temperatures of 295 and 11.4 K, using the GEM diffractometer[45] at the ISIS Facility, Rutherford Appleton Laboratory, Chilton, Didcot, UK, to provide data suitable for both Rietveld and total diffraction analysis. For both analysis methods, the absolute calibration of the detectors was achieved using diffraction data measured on crystalline $Y_3Al_5O_{12}$ (see Supporting Information, section S.5). Rietveld analysis of the diffraction patterns of $Zn(CN)_2$ was performed using GSAS software.[46,47] For total diffraction analysis, the corrected neutron interference function at each temperature, $Qi^N(Q)$ (Supporting Information Figure S.8), was Fourier transformed to obtain the differential neutron correlation function, $D^N(r)$ (Supporting Information Figure S.9), and the total neutron correlation function, $T^N(r)$ (Figure 7).

Total X-ray Diffraction Experiments. The X-ray diffraction pattern of $Zn(CN)_2$ was measured at 295 K, using a Panalytical X'Pert Pro Multipurpose diffractometer running in capillary mode, with a silver anode source ($\lambda = 0.560885$ Å) (see Supporting Information, section S.8). The corrected X-ray interference function $Qi^X(Q)$ (Supporting Information Figure S.8) was Fourier transformed to obtain the differential X-ray correlation function, $D^X(r)$ (Supporting Information Figure S.9), and the total X-ray correlation function, $T^X(r)$ (Figure 7).

■ ASSOCIATED CONTENT

ⓢ Supporting Information

Further details of the ^{67}Zn NMR experiments and quantum chemical calculations, together with additional PXRD and thermal expansion data, vibrational spectra, and details of total neutron and X-ray scattering analysis for $Zn(CN)_2$. This material is available free of charge via the Internet at http://pubs.acs.org.

■ AUTHOR INFORMATION

Corresponding Authors
s.j.hibble@rdg.ac.uk
a.m.chippindale@rdg.ac.uk
scott.kroeker@umanitoba.ca
alex.hannon@stfc.ac.uk

Present Addresses
$^{\perp}$Department of Chemistry and Francis Bitter Magnet Laboratory, Massachusetts Institute of Technology, Cambridge, Massachusetts 02139, United States.
$^{\#}$Faculty of Engineering, University of Nottingham, Nottingham NG7 2RD, United Kingdom.

Notes
The authors declare no competing financial interest.

■ ACKNOWLEDGMENTS

■ REFERENCES

(1) Goodwin, A. L.; Kepert, C. J. *Phys. Rev. B* **2005**, *71*, 140301R.
(2) Williams, D. J.; Partin, D. E.; Lincoln, F. J.; Kouvetakis, J.; O'Keeffe, M. *J. Solid State Chem.* **1997**, *134*, 164.
(3) Hoskins, B. F.; Robson, R. *J. Am. Chem. Soc.* **1990**, *112*, 1546.
(4) Chapman, K. W.; Chupas, P. J.; Kepert, C. J. *J. Am. Chem. Soc.* **2005**, *127*, 15630.
(5) Hibble, S. J.; Wood, G. B.; Bilbé, E. J.; Pohl, A. H.; Tucker, M. G.; Hannon, A. C.; Chippindale, A. M. *Z. Kristallogr.* **2010**, *225*, 457.
(6) Collings, I. E.; Cairns, A. B.; Thompson, A. L.; Parker, J. E.; Tang, C. C.; Tucker, M. G.; Catafesta, J.; Levelut, C.; Haines, J.; Dmitriev, V.; Pattison, P.; Goodwin, A. L. *J. Am. Chem. Soc.* **2013**, *135*, 7610.
(7) Werner-Zwanziger, U.; Chapman, K. W.; Zwanziger, J. W. *Z. Phys. Chem.* **2012**, *226*, 1205.
(8) Goodwin, A. L.; Calleja, M.; Conterio, M. J.; Dove, M. T.; Evans, J. S. O.; Keen, D. A.; Peters, L.; Tucker, M. G. *Science* **2008**, *319*, 794.

(9) Hibble, S. J.; Hannon, A. C.; Cheyne, S. M. *Inorg. Chem.* **2003**, *42*, 4724.

(10) Hibble, S. J.; Chippindale, A. M.; Pohl, A. H.; Hannon, A. C. *Angew. Chem., Int. Ed.* **2007**, *37*, 7116.

(11) Hibble, S. J.; Chippindale, A. M.; Bile, E. J.; Marelli, E.; Harris, P. J. F.; Hannon, A. C. *Inorg. Chem.* **2011**, *50*, 104.

(12) Chippindale, A. M.; Hibble, S. J.; Bilbé, E. J.; Marelli, E.; Hannon, A. C.; Allain, C.; Pansu, R.; Hartl, F. *J. Am. Chem. Soc.* **2012**, *134*, 16387.

(13) Tucker, M. G.; Goodwin, A. L.; Dove, M. T.; Keen, D. A.; Wells, S. A.; Evans, J. S. O. *Phys. Rev. Lett.* **2005**, *95*, 255501.

(14) Tucker, M. G.; Dove, M. T.; Keen, D. A. *J. Phys.: Condens. Matter* **2000**, *12*, L425.

(15) Tucker, M. G.; Dove, M. T.; Keen, D. A. *J. Phys.: Condens. Matter* **2000**, *12*, L723.

(16) Sears, V. F. *Neutron News* **1992**, *3*, 26.

(17) Nishikiori, S.; Ratcliffe, C. I.; Ripmeester, J. A. *Can. J. Chem.* **1990**, *68*, 2270.

(18) Ding, P.; Liang, E. J.; Jia, Y.; Du, Z. Y. *J. Phys.: Condens. Matter* **2008**, *20*, 275224.

(19) MacKenzie, K. J. D.; Smith, M. E. *Multinuclear Solid-State Nuclear Magnetic Resonance of Inorganic Materials*; Pergamon: Oxford, 2002.

(20) Wu, G. *Chem. Phys. Lett.* **1998**, *298*, 375.

(21) Ida, R.; Wu, G. *J. Phys. Chem. A* **2002**, *106*, 11234.

(22) Lipton, A. S.; Wright, T. A.; Bowman, M. K.; Reger, D. L.; Ellis, P. D. *J. Am. Chem. Soc.* **2002**, *124*, 5850.

(23) Lipton, A. S.; Heck, R. W.; Ellis, P. D. *J. Am. Chem. Soc.* **2004**, *126*, 4735.

(24) Lipton, A. S.; Heck, R. W.; Staeheli, G. R.; Valiev, M.; De Jong, W. A.; Ellis, P. D. *J. Am. Chem. Soc.* **2008**, *130*, 6224.

(25) Mroue, K. H.; Power, W. P. *J. Phys. Chem. A* **2010**, *114*, 324.

(26) Sutrisno, A.; Liu, L.; Xu, J.; Huang, Y. N. *Phys. Chem. Chem. Phys.* **2011**, *13*, 16606.

(27) Sutrisno, A.; Terskikh, V. V.; Shi, Q.; Song, Z. W.; Dong, J. X.; Ding, S. Y.; Wang, W.; Provost, B. R.; Daff, T. D.; Woo, T. K.; Huang, Y. N. *Chem.-Eur. J.* **2012**, *18*, 12251.

(28) Bak, M.; Rasmussen, J. T.; Nielsen, N. C. *J. Magn. Reson.* **2000**, *147*, 296.

(29) Reckeweg, O.; Simon, A. *Z. Naturforsch., B* **2002**, *57*, 895.

(30) Glusker, J. P.; Trueblood, K. N. *Crystal Structure Analysis: A Primer*, 2nd ed.; Oxford University Press: New York, 1985; p 176.

(31) Stout, G. H.; Jensen, L. H. *X-ray Structure Determination: A Practical Guide*, 2nd ed.; Wiley: New York, 1989; p 385.

(32) Busing, W. R.; Levy, H. A. *Acta Crystallogr.* **1964**, *17*, 142.

(33) Lorch, E. *J. Phys. C* **1969**, *2*, 229.

(34) Wright, A. C. In *Experimental Techniques of Glass Science*; Simmons, C. J., El-Bayoumi, O. H., Eds.; American Ceramic Society: Westerville, OH, 1993; p 205.

(35) Hannon, A. C.; Grimley, D. I.; Hulme, R. A.; Wright, A. C.; Sinclair, R. N. *J. Non-Cryst. Solids* **1994**, *177*, 299.

(36) It is important to note that when a peak in $T^N(r)$ can be ascribed to a unique atom pair, p and q, the distance derived from peak fitting is a model-independent measurement of the average instantaneous interatomic distance and does not depend on the many assumptions inherent in analyzing Bragg diffraction data using conventional crystallography.

(37) Mittal, R.; Zbiri, M.; Schober, H.; Marelli, E.; Hibble, S. J.; Chippindale, A. M.; Chaplot, S. L. *Phys. Rev. B* **2011**, *83*, 024301.

(38) Fairbank, V. E.; Thompson, A. L.; Cooper, R. I.; Goodwin, A. L. *Phys. Rev. B* **2012**, *86*, 104113.

(39) Goodwin, A. L.; Dove, M. T.; Chippindale, A. M.; Hibble, S. J.; Pohl, A. H.; Hannon, A. C. *Phys. Rev. B* **2009**, *80*, 054101.

(40) Ravindran, T. R.; Arora, A. K.; Sairam, T. N. *J. Raman Spectrosc.* **2007**, *38*, 283.

(41) Ravindran, T. R.; Arora, A. K.; Chandra, S.; Valsakumar, M. C.; Shekar, N. V. C. *Phys. Rev. B* **2007**, *76*, 054302.

(42) Eichele, K.; Wasylishen, R. E. WSOLIDS1 NMR simulation package, version 1.17.30, 2000.

(43) Frisch, M. J.; Trucks, G. W.; Schlegel, H. B.; Scuseria, G. E.; Robb, M. A.; Cheeseman, J. R.; Montgomery, J. A., Jr.; Vreven, T.; Kudin, K. N.; Burant, J. C.; Millam, J. M.; Iyengar, S. S.; Tomasi, J.; Barone, V.; Mennucci, B.; Cossi, M.; Scalmani, G.; Rega, N.; Petersson, G. A.; Nakatsuji, H.; Hada, M.; Ehara, M.; Toyota, K.; Fukuda, R.; Hasegawa, J.; Ishida, M.; Nakajima, T.; Honda, Y.; Kitao, O.; Nakai, H.; Klene, M.; Li, X.; Knox, J.; Hratchian, H. P.; Cross, J. B.; Bakken, V.; Adamo, C.; Jaramillo, J.; Gomperts, R.; Stratmann, R. E.; Yazyev, O.; Austin, A. J.; Cammi, R.; Pomelli, C.; Ochterski, J. W.; Ayala, P. Y.; Morokuma, K.; Voth, G. A.; Salvador, P.; Dannenberg, J. J.; Zakrzewski, V. G.; Dapprich, S.; Daniels, A. D.; Strain, M. C.; Farkas, O.; Malick, D. K.; Rabuck, A. D.; Raghavachari, K.; Foresman, J. B.; Ortiz, J. V.; Cui, Q.; Baboul, A. G.; Clifford, S.; Cioslowski, J.; Stefanov, B. B.; Liu, G.; Liashenko, A.; Piskorz, P.; Komaromi, I.; Martin, R. K.; Fox, D. J.; Keith, T.; Al-Laham, M. A.; Peng, C. Y.; Nanayakkara, A.; Challacombe, M.; Gill, P. M. W.; Johnson, B.; Chen, W.; Wong, M. W.; Conzalez, C.; Pople, J. A. *Gaussian 03*, Revision C.02; Gaussian, Inc.: Pittsburgh, PA, 2003.

(44) Segall, M. D.; Lindan, P. J. D.; Probert, M. J.; Pickard, C. J.; Hasnip, P. J.; Clark, S. J.; Payne, M. C. *J. Phys.: Condens. Matter* **2002**, *14*, 2717.

(45) Hannon, A. C. *Nucl. Instrum. Methods Phys. Res., Sect. A* **2005**, *551*, 88.

(46) Larson, A. C.; Von Dreele, R. B. Los Alamos Report, LAUR 86-748, 2004.

(47) Toby, B. H. *J. Appl. Crystallogr.* **2001**, *34*, 210.

16489

dx.doi.org/10.1021/ja406848s | *J. Am. Chem. Soc.* 2013, 135, 16478−16489